Title: Estimation of Dynamic Interstory Drift in Buildings using Wireless Smart Sensors

Fernando Gomez;[a] Yuguang Fu,[b*] M. ASCE; Tu Hoang;[c] Kirill Mechitov;[d] Billie F. Spencer, Jr.[e] F. ASCE

Abstract

Interstory drift response is one of most important quantities to quickly assess performance and damages in buildings. Nevertheless, direct measurement of interstory drift is difficult and expensive, because a stationary reference is required to attach measurement devices. With the goal of accurate and fast reference-free estimation, this paper proposes a new strategy to determine dynamic interstory drifts using accelerations. In particular, a Tikhonov regularization is adopted in a generalized minimization problem to achieve an efficient and stable FIR filter. Furthermore, due to independent clocks in wireless sensors, accurate time synchronization of the records is critical, and consequently, a strategy for accurate synchronization is also presented. Finally, the proposed strategy has been deployed on edge devices for onboard real-time interstory drift estimation. The proposed method for dynamic interstory drift estimation is validated, first, by numerical simulation using earthquake records as base excitation of linear and nonlinear buildings, as well as through laboratory shake table experiments. Both numerical and lab test results show good agreement of dynamic interstory drifts between the measured value and estimated results, demonstrating the efficacy of the proposed method to estimate the dynamic displacements of seismically excited structures.

KEYWORDS: Reference-free displacement estimation, smart wireless sensor, FIR filter, time synchronization.

---

[a] Professor, College of Science and Engineering, Universidad San Francisco de Quito, Brillat-Savarin Building, BS-216, Diego de Robles s/n, Quito 170901, Ecuador

[b] Assistant Professor, School of Civil and Environmental Engineering, Nanyang Technological University, 50 Nanyang Ave, 639798, Singapore (Corresponding author, yuguang.fu@ntu.edu.sg)

[c] Structural Engineer, Geocomp, 125 Nagog Park, Acton, MA 01720, USA

[d] Chief Technology Officer, Embedor Technologies, 60 Hazelwood Dr. Champaign, IL 61801, USA

[e] Nathan M. & Anne M. Newmark Endowed Chair in Civil Engineering, Department of Civil and Environmental Engineering, University of Illinois at Urbana-Champaign, 205 N. Matthews Ave., Urbana, IL 61801, USA

1. INTRODUCTION

Measurement of structural displacements under service or extreme loads are typically desired for applications such as calibrating structural designs and assessing structural performance (Skolnik and Wallace, 2010). Furthermore, buildings interstory drifts are recognized as a critical quantity to estimate structural performance and damage (Bennett and Batroney, 1997). Direct measurement of interstory drift is difficult because it is the difference of displacement between two stories, e.g., using linear variable differential transformers and laser-based sensors (Islam et al, 2016). Alternatively, displacement measurements can be obtained directly by non-contact sensors from a remote location, e.g., using laser Doppler vibrometers which can be quite expensive (Kim and Sohn, 2017). Recently, computer vision systems, such as commercial grade cameras/smartphones or unmanned aerial systems has received increasing attention. However, they usually require a reference on the video which may not be readily available (Luo and Feng, 2018; Lee et al, 2020). In addition, the sampling frequency is limited by the typically low camera frame rate, the visibility is governed by environmental and lighting conditions, and the accuracy is affected by long distances from the viewpoint to the region of interest. Note that the existing solutions are not well-suited for interstory drift measurement of real-scale buildings as either the cost are prohibitive, a reference is needed, or implementation is challenging.

Researchers have proposed to calculate interstory drifts indirectly from estimated displacement using other measurements such as velocities, accelerations, and/or strains. Estimation using accelerations has good potential because of the ease and low cost to measure accelerations reliably. However, displacement estimation using double integration diverges, because it amplifies the noise in the acceleration, especially in low-frequency domain. Many solutions have been proposed for this problem (Kim et al, 2014; Nagayama et al, 2017; Hester et al, 2017; Abé and Fujino, 2017; Gindy et al, 2008; Liu et al, 2017). For example, a recursive high-pass filter and a recursive integrator are proposed to achieve real-time online displacement estimation by means of multi-round baseline correction, filtering, and integration (Zheng et al, 2019). This method has yet to be implemented in edge devices for real-time demonstration. An extended Kalman filter with an embedded Bayesian noise-parameter updating has also been proposed to reduce numerical errors in displacement estimation from seismic accelerations. However, it requires a nonlinear model, which may not be available for many scenarios (Pan et al, 2021). To improve the accuracy, the author has proposed an approach to minimize the L2-norm of a functional with a Tikhonov regularization, which represents a higher-order derivative of the difference of the measured acceleration and the second derivative of the estimated displacement (Gomez et al, 2018). On the other hand, the residual deformation, corresponding to the DC component in the frequency domain, is not able to be captured by integrating. To address this concern, many researchers consider data fusion, leveraging another type of sensors which can capture the low-frequency component and stitching it together with the information obtained from accelerometers (Park et al, 2013; Zhu et al, 2020; Park et al, 2018; Kim et al, 2018). This paper is focused on deployment scenarios where only accelerometers are available, which is very common for full-scale deployment of wireless smart sensors in buildings. Indeed, acceleration is the most reliable and popular measurement, mainly because accelerometers are easy to install and do not require complex surface mounting.

In this paper, the goal is to estimate interstory drift from acceleration-only measurements using wireless smart sensors, with a focus on time synchronization while comparing displacement estimation from different sensors. Wireless smart sensors (WSS) are cost-effective small-size integrated data acquisition devices, which consist of sensors (most often accelerometers), computing unit, wireless transceiver, and/or actuation interface (Lynch et al, 2006; Rawat et al, 2014). Major efforts have been spent on developing WSS prototypes with advancements both in hardware and software, e.g., iMote2 and Xnode developed by researchers from University of Illinois (Rice et al, 2010; Rice et al, 2011; Jo et al, 2011; Spencer et al, 2017; Fu et al, 2016; Fu et al, 2019). While efficient for displacement estimation, WSS have several inherent challenges that must be addressed, one of which is time synchronization. In particular, WSS use local clocks, which do not share a global time and they drift at different rates. Furthermore, synchronization of local clocks of different sensor nodes does not guarantee the synchronization of measurement data obtained from each sensor node (Nagayama and Spencer, 2007). The usage of unsynchronized data may negatively affect subsequent analysis, especially for interstory drift estimation, which relies on the relative displacement estimations between each pair of sensors. Though some studies have developed and implemented the technologies of time synchronization on several WSS platforms (Wang et al, 2007; Kim et al, 2010; Bocca et al, 2011), most of the work solely considers clock and not data synchronization.

This study proposes the use of a FIR filter via Tikhonov regularization to estimate accurate dynamic interstory drifts in buildings based on acceleration measurements at different floors. Furthermore, an efficient time synchronization strategy is proposed to enable the usage of wireless smart sensors to obtain accurate dynamic interstory drift estimation. The filter method together with the time synchronization strategy is finally deployed on a network of WSS and executed onboard using limited computational resources.

2. DYNAMIC INTERSTORY DRIFT ESTIMATION FROM ACCELERATION RECORDS

The use of Tikhonov regularization to estimate dynamic displacements was first proposed by Hong's group (Hong et al, 2010; Lee et al, 2010), and subsequently improved by Gomez et al (2018) to estimate dynamic reference-free bridge displacements. Among other dynamic displacement estimation algorithms, it gives the best accuracy, introduce zero phase delays in the measurement, and calculates the results in an efficient time. Therefore, this idea is adopted in this study in buildings to estimate dynamic interstory drifts. For the convenience of the reader, a brief overview of the filter formulation is presented in the following subsection.

2.1 Displacement estimation formulation

The following functional with Tikhonov regularization represents the error in a high-order derivative of the difference between estimated displacements and measured accelerations (Gomez et al, 2019),

$$\Pi(u)=\frac{1}{2}\int_T\left[\frac{d^{n-2}}{dt^{n-2}}\left(\frac{d^2u}{dt^2}-\bar{a}\right)\right]^2 dt+\frac{1}{2}\beta^n\int_T u^2dt \tag{1}$$

where T is the time window of interest $t_1<t<t_2$, $\bar{a}$ is the measured acceleration, u is the estimated displacement, $n\geq 2$ is an integer named as the order of the functional, and $\beta>0$ is a parameter known as the factor of Tikhonov regularization.

From the previous functional, the following ordinary differential equation is obtained based on the variational calculus.

$$\frac{d^{2n}u}{dt^{2n}}+(-\beta)^n u=\frac{d^{2n-2}\bar{a}}{dt^{2n-2}},\quad t_1<t<t_2 \tag{2}$$

To achieve a unique solution, the boundary conditions (BC) for the differential equation are known displacements and derivatives at the ends of the time window t_1,t_2. However, these BC are not available for this application. Although, the BC affect the solution close to ends of the time window, their influence is smaller towards the center of the time window. Consequently, using superposing moving windows centered at each time point minimize the effect of the unknown BC.

Following the Fourier transform of the differential equation, the frequency response is obtained.

$$H_{u\bar{a}}(\omega) = -\frac{\omega^{2n-2}}{\omega^{2n} + \beta^n} \tag{3}$$

The regularization factor β is computed by defining a target frequency f_T and target accuracy α_T, obtaining the following expression.

$$\beta = \sqrt[n]{\frac{1-\alpha_T}{\alpha_T}}(2\pi f_T)^2 \tag{4}$$

The previous continuous-time representation is unstable, therefore, a discrete FIR filter is considered instead, a FIR filter of type I with generalized linear phase is chosen. The FIR filter is represented by a vector of coefficients **c** with the length of 2k+1. Consequently, the estimated displacement is given in terms of the measured acceleration and the FIR filter by the formula

$$u(t) = (\Delta t)^2 \sum_{p=-k}^{k} c_{k+1+p}\bar{a}(t + p\Delta t) \tag{5}$$

where the coefficients of filter are given by

$$c_{p+k+1} = -\frac{f_s}{2\pi^2}\int_0^{f_s/2} \frac{f^{2n-2}}{f^{2n} + \lambda^{2n} f_T^{2n}} \cos(2\pi p f \Delta t)\, df \tag{6}$$

The filter length is determined by the normalized window length N_w, the target frequency f_T, and the sampling frequency f_s, expressed as,

$$k = N_w \frac{f_s}{2 f_T} \tag{7}$$

The normalized time window is defined, so as to make the impulse response function end at zeros in both ends, which minimizes Gibbs' phenomenon and rippling in the frequency domain. Appropriate values for the normalized window length N_w are presented in (Gomez et al, 2019).

2.2 FIR filter for interstory drift estimation

To estimate dynamic interstory drifts, acceleration records two consecutive floors are required: $\bar{a}_i$ and $\bar{a}_{i+1}$. The measurements need to be synchronized in time and have the same sampling frequency. For wired sensors, time synchronization is not a problem even for long cables, but in wireless smart sensors, it is a major challenge to overcome. Section 3 describes the details of this problem and a solution strategy.

The dynamic interstory drifts are estimated using the FIR filter proposed in the previous section, which is defined by the vector of coefficients **c**. Consequently, the estimated displacements at the two locations are given in terms of the measured accelerations and the FIR filter by the formula

$$u_i(t) = (\Delta t)^2 \sum_{p=-k}^{k} c_{k+1+p} \bar{a}_i (t + p\Delta t) \tag{8}$$

$$u_{i+1}(t) = (\Delta t)^2 \sum_{p=-k}^{k} c_{k+1+p} \bar{a}_{i+1} (t + p\Delta t) \tag{9}$$

where the coefficients of filter are given by Eq. (6) and the filter length is given by Eq. (7).

The same FIR filter is used at both locations which come from the same structure, and both acceleration records assume to use the same sampling rate. Therefore, the estimated interstory drift is determined by the difference of these displacement values from acceleration records.

$$\theta_i(t) = u_{i+1}(t) - u_i(t) = (\Delta t)^2 \sum_{p=-k}^{k} c_{k+1+p} \left[\overline{a}_{i+1}(t + p\Delta t) - \overline{a}_i(t + p\Delta t) \right] \tag{10}$$

$$\theta_i(t) = (\Delta t)^2 \sum_{p=-k}^{k} c_{k+1+p} \Delta\overline{a}_i(t + p\Delta t) \tag{11}$$

where $\Delta\overline{a}_i = \overline{a}_{i+1} - \overline{a}_i$ is the relative acceleration of consecutive floors.

The filter coefficients need to be computed only once at the beginning. In addition, the proposed method requires the multiplication of two vectors, coefficients and acceleration, to estimate interstory drifts at each time step. However, this filter is not causal, as it requires the measured relative accelerations of *k* points in the future. Then, this estimation is obtained with a time delay equal to half the time window length; however, this would typically lead to small lags in the estimation, and it can be implemented in near-real time.

3. WIRELESS SMART SENSORS AND TIME SYNCHRONIZATION

This section presents the details about wireless smart sensors and strategies for time synchronization of the time records. The proposed method is deployed in wireless smart sensors for estimating dynamic interstory drifts, and time synchronization between different sensors is addressed by a two-point two-stage strategy proposed by the authors.

3.1 High-fidelity sensor platform

To provide high-quality measurement and high-efficiency processing for drift estimation, this study leverages a next-generation wireless smart sensor platform, the Xnode (Fig. 1)

(Spencer et al, 2017), because of its excellent features both in hardware and software. In particular, the Xnode employs an 8-channel, 24-bit analog-to-digital converter, which enables high-resolution data collection at a high sampling rate of up to 16kHz. In addition, the Xnode features a powerful microprocessor that operates with a dual Cortex core at frequencies up to 204MHz, suitable for data-intensive on-board computation, like the interstory drift estimation. On the software side, in contrast to most commercial WSS, the Xnode is open-source, allowing users to modify and customize the software and applications. Moreover, the Xnode retains much of the successful SOA-based middleware of the Illinois Structural Health Monitoring Services Toolsuite (Rice et al, 2010) and implements it in a preemptive multitasking framework using the standard C programming language (Fu et al, 2016), which significantly facilitates the end-user development. More comprehensive performance efficacy and discussion of the Xnode can be found in the paper (Fu et al, 2018; Fu et al, 2019). Xnode smart sensor is leveraged in this study for deployment and evaluation of interstory drift estimation. Fig. 1 shows the hardware and software details of the Xnode smart sensor.

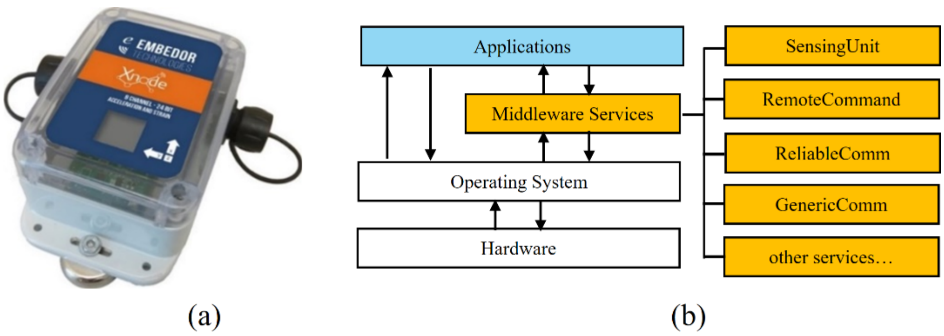

Fig. 1. Xnode smart sensor: (a) hardware platform, (b) software framework

3.2 Two-point two-stage time synchronization for interstory drift estimation

To address the challenge of time synchronization between wireless smart sensors, an efficient strategy, named as two-point two-stage time synchronization, is proposed for interstory drift estimation. The two stages include clock and data synchronization. This section provides a brief description of the development and implementation of this strategy.

To prepare for the time synchronization strategy, lab tests were first conducted to quantify the clock drift behavior of wireless smart sensors, Xnodes in this study. The test results reveal that, without time synchronization, a drift rate achieves up to 13 μs/s, while nonlinear drift behavior is negligible and sampling rate is stable (Fu et al., 2021a). Based on the observations, an efficient two-point clock synchronization is developed, as shown in Fig. 2. Specifically, before sensing starts, a series of beacons with global time stamps are broadcasted from the gateway node to sensor nodes at an interval of 1 ms. Upon reception of beacons, each sensor node records the local clock and obtain a series of corresponding clock offsets. The medium value of these offsets is selected as the 1st Point of clock information before sensing starts. Specifically, in this process, up to 10 beacons at 5-millisecond intervals were exchanged between the gateway node and all the sensor nodes to obtain the clock offsets before sensing (1st point), recorded as $\Delta t_j(i)$,

$$\Delta t_j(i) = t_{lbj}(i) - t_{gbj}(i), \quad i \in [1,9] \tag{12}$$

Where $t_{gb}(i)$ is transmission time of beacon i, recorded in the gateway node, and $t_{lb}(i)$ is reception time, recorded in the sensor nodes. After at least five offset values are given, the median of the offset values, Δt_1, and associated local clock, t_1, are used as the clock information pair for the current round of point synchronization. In the meantime, the current clock offset is compensated, such that all the sensor nodes start sensing approximately at the same designated time, T_{start}. In addition, the time to stop sensing is obtained as $T_{\text{stop}} = T_{\text{start}} + T_{\text{sensing}}$, where T_{sensing} is specified by users. During sensing, the updated local clock is recorded when sensing starts and stops, labeled as t_{start} and t_{stop}, respectively.

After sensing stops, similarly, another round of clock offset investigation is carried out, and the 2nd Point of clock information obtained. Afterwards, clock drift is estimated based on clock offsets obtained in the 1st Point and the 2nd Point,

$$k = (\Delta t_2 - \Delta t_1)/(t_2 - t_1), \quad b = \Delta t_2 \tag{13}$$

which are used to correct the time stamp t_{lb} in each sensor node as

$$t'_{lb} = t_{lb} - b - k(t_{lb} - t_2) \tag{14}$$

In addition, we can obtain the offset of start-up sensing time in Eq. (15), which will be further used for the next step of data synchronization process.

$$dt = \frac{1}{2}\left(T_{\text{start}} + T_{\text{stop}} - t_{\text{start}} - t_{\text{stop}}\right) \tag{15}$$

Finally, a resampling-based approach developed by Nagayama and Spencer (2007) is applied to achieve data synchronization. It will address three uncertainties for synchronization:

offset in start-up time, sampling rate difference among sensor nodes, and sampling rate fluctuation in a single node. For the completeness of the methodology, a brief discussion about this approach is conducted next. The basic idea of resampling is to achieve a signal with a factor of L/M, via upsampling by L, filtering, and downsampling by M. In the process, a polyphase implementation is applied to simplify the execution of an FIR filter. For a non-integer downsampling factor of M to achieve a precise sampling rate, the introduction of an initial delay (before upsampling and linear interpolation) is applied in the downsampling process. assuming that the output data points do not necessarily correspond to the points on the upsampled signal. For data synchronization, the entire sampling dataset is divided into several blocks. In each block, the offset of starting time (i.e., first data point) is estimated first; and the actual sampling rate is also calculated by $(t_{\mathrm{current}} - t_{\mathrm{last}})/N$. The timestamps after clock synchronization are then used to obtain the misalignment of sample points. Finally, resampling is applied to each block of data.

In summary, combining clock synchronization and data synchronization is proposed. This strategy achieves time synchronization in an efficient way, whilst compensating the effect of nonlinear clock drift. Compared with conventional methods, it is effective and accurate, which is suitable for interstory drift estimation in this study. Laboratory tests were conducted to evaluate the precision of the proposed approach, using three sensor nodes as leaf nodes and one gateway node. The pairwise synchronization errors are collected and averaged for comparison.

Table 1 presents the comparison of precision between the proposed approach and the state-of-the-art solutions in the literature. The reference data is collected from the literature (Li et al., 2016), consisting of post-sensing time synchronization with linear and nonlinear regressions. It should be noted that, the difference of precision may be due to both hardware and approaches. It demonstrates that the proposed two-point two-stage effective time synchronization can achieve a time synchronization error of less than 15 μs, which is sufficiently precise for the SHM applications in this study.

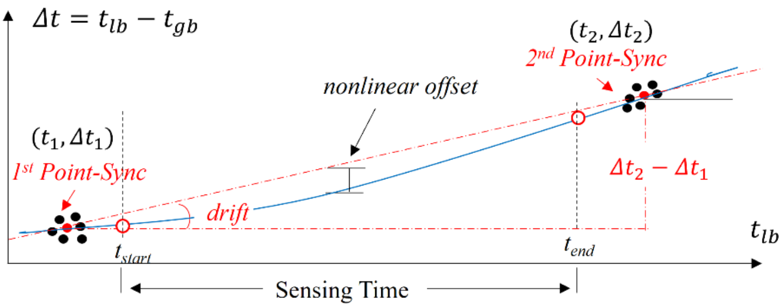

Fig. 2. The proposed time synchronization: clock synchronization illustration

Table 1. Comparison of time synchronization errors

Sensing duration	Pairwise synchronization error (mean value, μs)		
	Post-sensing time synch with linear regression	Post-sensing time synch with nonlinear regression	The proposed approach
1min	18.63	18.26	7.46
10min	18.33	17.86	6.44
30min	17.63	13.27	11.48

4 NUMERICAL VALIDATIONS

This section considers three examples as numerical validation of the approach for linear and nonlinear buildings subjected to different excitations. In real applications, nonlinear behavior, such as yielding or nonlinear restoring forces, is expected in building components, and therefore, the examples show the performance of the proposed method in linear buildings, nonlinear hysteretic buildings, and linear building with nonlinear protection devices.

4.1 Linear 9-story building

In this section, a benchmark example is considered, where a 9-story linear shear building is modeled subjected to ground motions (Xu et al, 2017), to numerically evaluate the accuracy of the method. In particular, the mass is 505×10^3 kg for the first floor, 495×10^3 kg for the second to eighth floors, and 535×10^3 kg for the roof, respectively. The stiffnesses is 600, 578, 544, 502, 453, 397, 332, 256, and 162 MN/m for the first to the last floor, respectively. The modal damping ratio is 2% for all the modes. Regarding the excitations, we consider two different ground motions, including El Centro (EC) earthquake record, and an artificial earthquake which is processed by the non-stationary Kanai-Tajimi (NSKT) model (Xu et al, 2017) with the properties including $\omega_{\mathrm{g}}=12$ rad/s, $\zeta_{\mathrm{g}}=0.3$, $S_0=0.02$ m^2/s^3, and $e(t)=4\left(e^{-0.1t}-e^{-0.2t}\right)$.

The numerical model is built and executed with a sampling rate of 1000 Hz in MATLAB Simulink, and the collected response datasets are then down-sampled to the frequency of 100 Hz to match the popular sampling rate of wireless smart sensors (e.g., Xnodes). All interstory drifts are computed for comparison purposes. All floor accelerations and base acceleration are measured. To make it more realistic, datasets are added with a zero-mean Gaussian noise, where standard deviation is equal to 5% of the maximum RMS acceleration. this noise magnitude has been chosen based on similar previous studies (Park et al., 2018; Gomez et al., 2019).

We use the proposed method to estimate the dynamic interstory drift in all floors using the relative accelerations, using the following parameters: $f_s = 100$ Hz, $n = 4$, $f_T = 0.8$ Hz, $\alpha_T = 0.99$, and $N_w = 5.223$. The total interstory drift is considered as a reference for comparison, this is because in the measurements, the pseudo-static components are very small and no need to extract the dynamic counterparts. Fig. 3 and 4 show the interstory drifts of floors 1 and 6 subjected to ground motions EC and NSKT, respectively. These figures demonstrate that the obtained drifts match well with the exact values for all time steps.

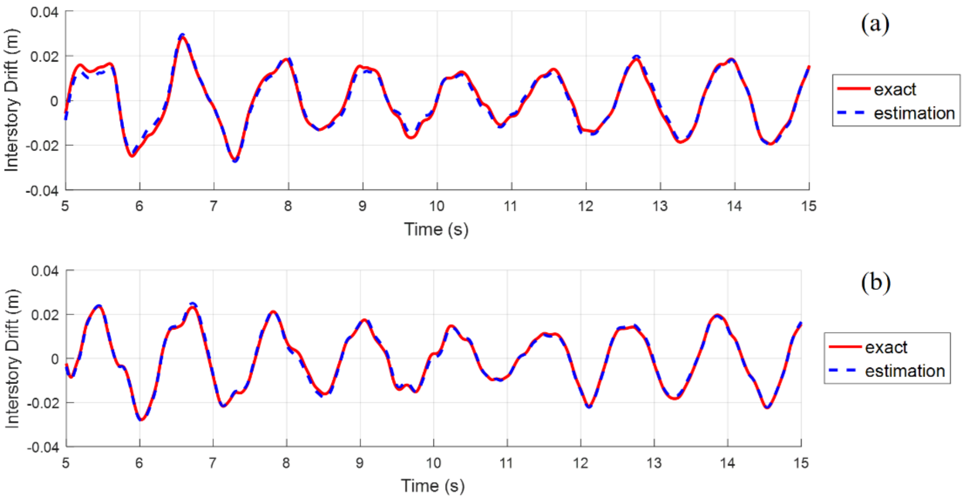

Fig. 3. Comparison of interstory drifts under EC ground motion: (a) first story and (b) sixth story

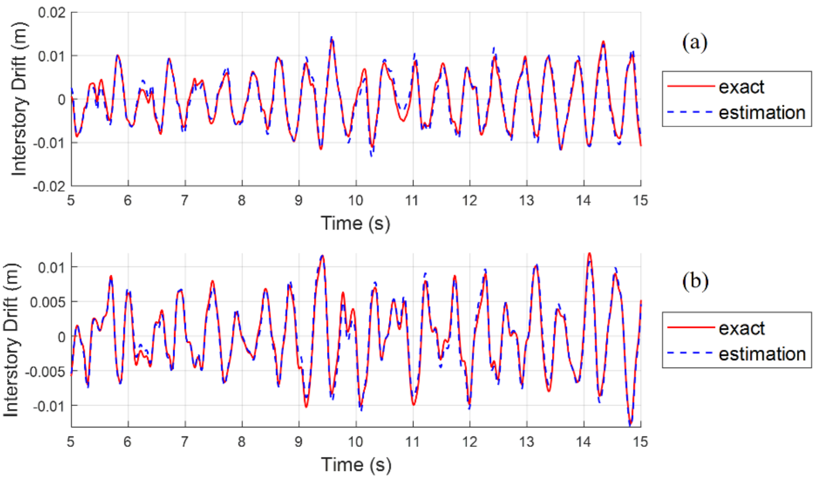

Fig. 4. Comparison of interstory drifts under NSKT ground motion: (a) first story and (b) sixth story

In particular, two types of error metrics are obtained to assess the accuracy of the proposed method: the amplitude error and the RMS error. The amplitude error is given as the difference between the maximum estimated value and the maximum exact value divided by the maximum exact value. In earthquake engineering, the maximum interstory drift is one of the most important metrics (Bennett and Batroney, 1997). The magnitude of the amplitude error represents an important metric in the accuracy of the maximum interstory drift. The RMS error is defined by the root-mean-square of the difference between the estimated value and the exact value divided by the maximum exact value. Table 2 lists both types of errors under the two excitations. It demonstrates that the errors are relatively small although introducing relatively large Gaussian noise. It is also observed that, the estimations under the NSKT ground motion have larger errors than those under EC, which can be explained as the largest response occurs in one floor but all records are polluted using the Gaussian noise with the same amplitude using only the RMS of the maximum response. In the experiments, the measurement noise in acceleration measurements should be smaller than assumed values in the numerical examples.

Table 2. Estimation errors of dynamic interstory drifts in the linear 9-story building

Story	El Centro		Non-stationary Kanai-Tajimi	
	Amplitude Error (%)	**RMS Error (%)**	**Amplitude Error (%)**	**RMS Error (%)**
1	4.89	3.42	1.26	6.17
2	2.03	3.75	6.30	6.98
3	4.77	4.30	2.36	7.99
4	4.73	3.47	1.37	9.59
5	1.43	4.29	1.60	8.37
6	1.17	3.31	6.08	6.94
7	1.02	2.83	7.04	4.46
8	5.38	2.89	2.82	4.30
9	0.79	2.87	5.97	3.22

As discussed in Section 1, measurements from different wireless smart sensors have time lags between them. Now, to assess the effect of this issue in the estimation, a time lag of 10 milliseconds is introduced in the acceleration record of the sixth floor. Clearly, this change will greatly affect the interstory drift of the sixth and seventh floor.

Fig. 5 shows the comparison of the interstory drift for 6th floor for both ground motions. The estimated and exact values do not agree as well as before. The time lag in the data harms the accuracy of the method. Smaller time lags need to be assured to achieve good results as before.

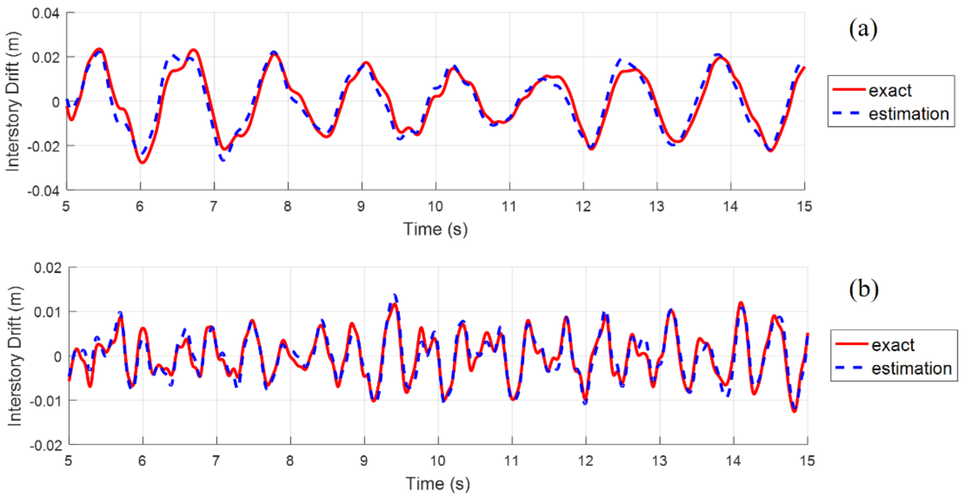

Fig. 5. Comparison of interstory drifts for sixth story with a time lag of 10 ms: (a) EC and (b) NSKT ground motions

Table 3 shows the amplitude and RMS error for both excitations. The amplitude errors are slightly larger but do not change much from the previous case. However, the RMS error is considerably amplified because the time lag not only affects the amplitude but also introduces a lag between the estimation and exact measurements. In sum, a strategy to limit time lags in data from different wireless sensors is needed to achieve good accuracy in the drift estimation.

Table 3. Estimation errors with a time lag of 10 milliseconds at sixth floor acceleration

Story	El Centro		Non-stationary Kanai-Tajimi	
	Amplitude Error (%)	RMS Error (%)	Amplitude Error (%)	RMS Error (%)
6	1.64	13.13	5.53	15.44
7	10.64	12.14	11.03	8.09

4.2 Nonlinear 3-story building

A 3-story nonlinear hysteretic shear building is applied in this section to test the accuracy of the method, subjected to ground motions (Xu et al, 2017). The mass of each floor is 6000 kg. The linear stiffnesses for the first to the last floor are 2.178, 1.772, and 1.2969 MN/m, respectively. The damping ratios are assumed to be 1.6%, 1.7%, and 2.7% for each mode. Each floor is considered as an elastoplastic element with smooth transition using Bouc-Wen hysteretic behavior; typical parameters are assumed for each floor: $\gamma = \beta = 0.5,\ A = 1,\ n = 1,\ \alpha = 0.04,\ d_y = 0.01$. Two ground motions are considered: El Centro (EC) earthquake record scaled to 20% and with no scaling; for larger amplitudes of the record, the response should have a larger nonlinear component. The excitation, Simulink simulation, and data post-processing are the same as those set in Section 4.1.

In this case, the elastoplastic behavior implies residual deformation due to yielding in the system and this phenomenon introduces pseudo-static displacements; this phenomenon increases as the amplitude of the excitation is increased. Therefore, the dynamic interstory drift is extracted from the measured total interstory drift to provide a comparison with the estimated interstory drift. Fig. 6 shows the total and dynamic interstory drifts of the first story for both excitations. It should be clarified that, for strong earthquakes, the response is expected to consist of large residual deformations; however, the dynamic interstory drift is still considered useful for rapid condition assessment of buildings (Fu et al, 2021b). Other types of nonlinear behavior such as components with nonlinear restoring forces do not introduce residual deformations and the total interstory drift can be recovered with the proposed method; this case is presented in the next subsection.

The proposed method is applied to estimate dynamic interstory drifts using measured accelerations, and it considers the following parameters: $f_s = 100$ Hz, $n = 4$, $f_T = 1.2$ Hz, $\alpha_T = 0.99$, and $N_w = 5.223$. Fig. 7 and 8 show the comparison of the dynamic interstory drift for floors 1 and 2 and for both excitations. As these figures show, the estimated interstory drift agrees well with exact dynamic interstory drift for all time steps. Table 4 shows the amplitude and RMS errors of interstory drift estimation for both excitations. As can be seen in the figure, the errors between the estimated and the exact dynamic interstory drifts are relatively small.

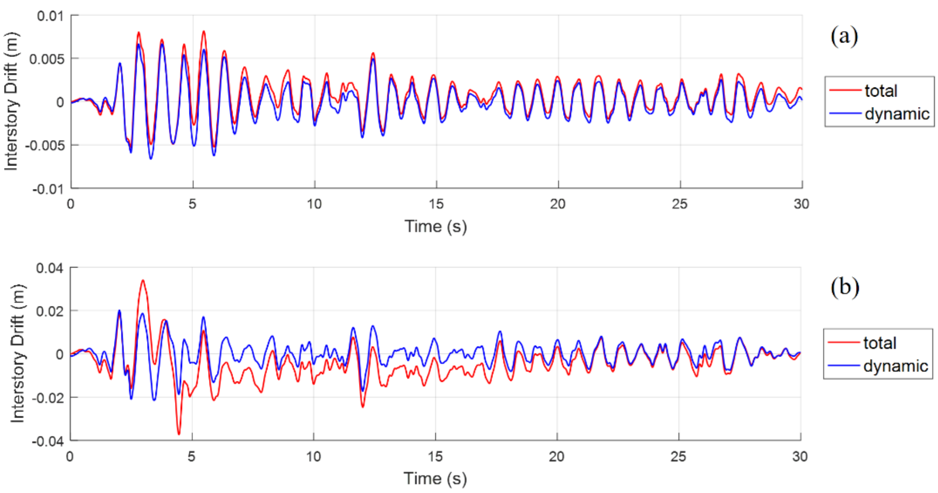

Fig. 6. Total and dynamic interstory drifts of the first story with EC (a) scaled to 20% and (b) unscaled

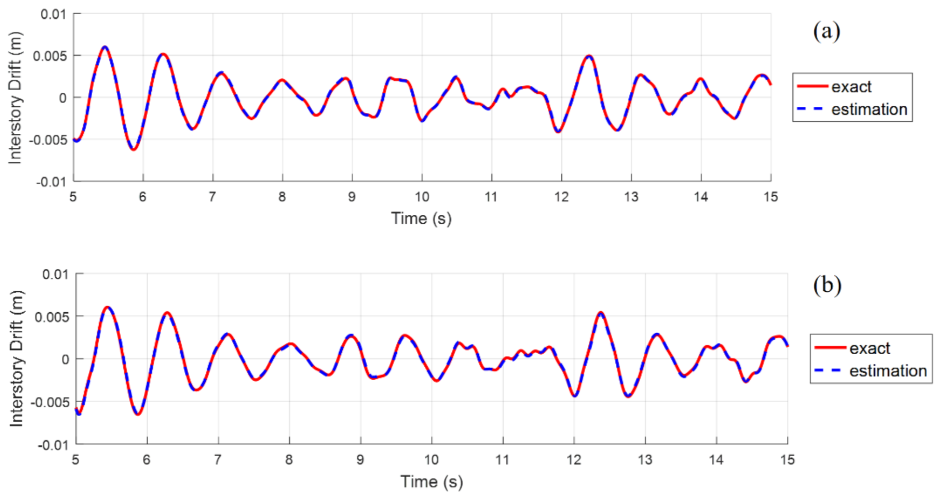

Fig. 7. Comparison of interstory drifts with EC scaled to 20%: (a) first and (b) second story

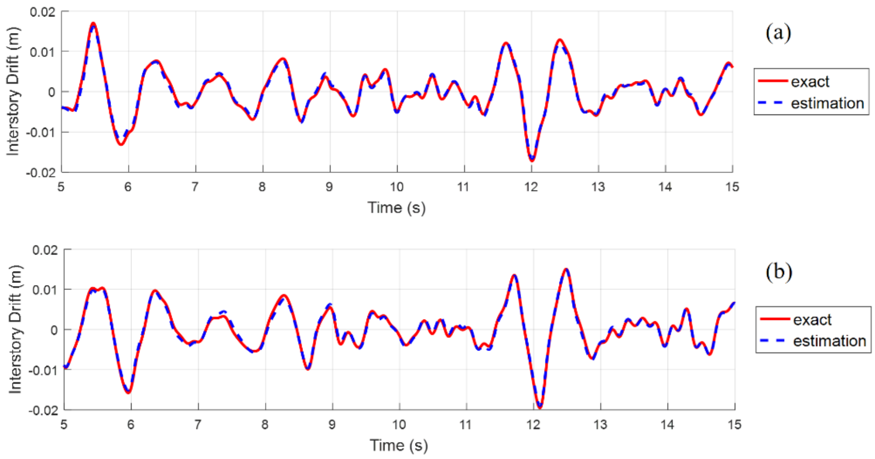

Fig. 8. Comparison of interstory drifts with EC unscaled: (a) first and (b) second story

Table 4. Estimation errors of dynamic interstory drifts in the nonlinear 3-story building

	El Centro 20%		El Centro 100%	
Story	Amplitude Error (%)	RMS Error (%)	Amplitude Error (%)	RMS Error (%)
1	2.40	1.31	3.79	2.56
2	0.05	1.44	3.01	2.11
3	1.12	1.74	0.90	3.12

To study the effect of nonlinear effects on the accuracy of the proposed method for total interstory drifts, the analysis was performed for different scalings of El Centro. The magnitude error and RMS error for the different scaling are shown in Fig. 9. Both types of errors increase as the nonlinear behavior increases. Moreover, unless large nonlinear plastic behavior, which achieves residual deformations, is expected to occur, the error in the estimated interstory drift with respect to the total interstory drift is reasonable.

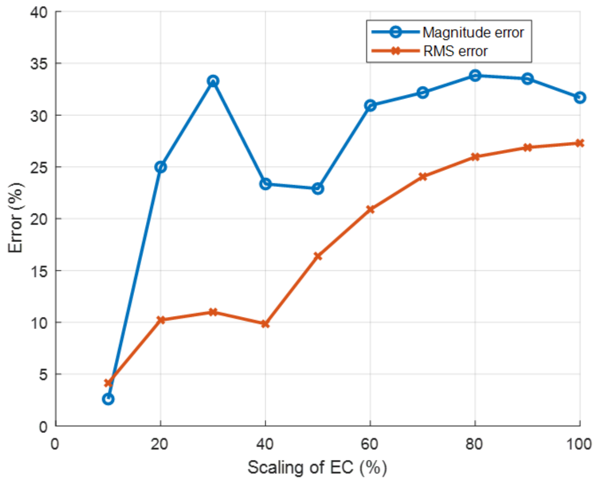

Fig. 9. Comparison of errors for the total interstory drifts of the first floor for different levels of EC

4.3 Linear 2-story building with a nonlinear energy sink

Buildings with seismic protective devices such as nonlinear dampers or isolators typically have a nonlinear behavior with limited pseudo-static residual deformations, and interstory drift measurement of these nonlinear systems is of interest as well. This example is representative of buildings with non -linear protection devices. A 2-story linear shear building with a nonlinear energy sink (NES) on the roof subjected to ground motions (Gomez et al, 2021) is considered as an example of these systems. In this case, the device stroke, which is the relative displacement of the floor and the device, is also a response of interest.

The masses of the floors are 24.3 and 24.2 kg. The linear stiffnesses are 6820 and 8220 N/m. The damping ratios are assumed to be 0.1% for the two modes of the uncontrolled structure. The NES in the roof is a Duffing oscillator without a linear term with mass equal to 6.81% of the total mass, linear damping force with constant 3.57 N-s/m, and the coefficient $\alpha_N = 63.97$ m^{-3} [34]. Two ground motions are considered: EC earthquake record and NSKT model with the following properties: $\omega_\mathrm{g} = 20.3$ rad/s, $\zeta_\mathrm{g} = 0.32$, $S_0 = 0.026$ m^2/s^3, and $e(t) = 4\left(e^{-0.1t} - e^{-0.2t}\right)$ (Gomez et al, 2021). Due to the essential nonlinearity in the NES, the system always has a nonlinear behavior. The excitation, Simulink simulation, and data post-processing are the same with those set in Section 4.1.

The proposed method is applied to estimate dynamic interstory drifts from measured accelerations with the following parameters: $f_\mathrm{s} = 100$ Hz, $n = 4$, $f_T = 1.0$ Hz, $\alpha_T = 0.99$, and $N_\mathrm{w} = 5.223$. The total interstory drift is considered as a reference for comparison, this is because in the measurements, the pseudo-static components are very small and no need to extract the dynamic counterparts. Fig. 10 and 11 show the comparison of the interstory drift for the first floor and device stroke subjected to ground motions EC and NSKT, respectively. It can be demonstrated that the estimated drifts agree well with the exact values. Table 5 shows both types of errors for both excitations. It demonstrates that the errors are relatively small although relatively large Gaussian noise are introduced.

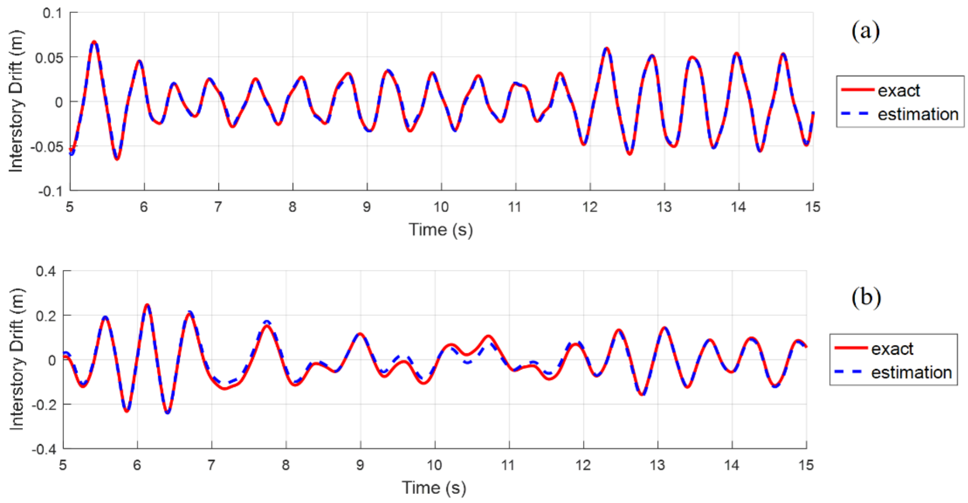

Fig. 10. Comparison with EC for (a) interstory drift of first floor and (b) device stroke

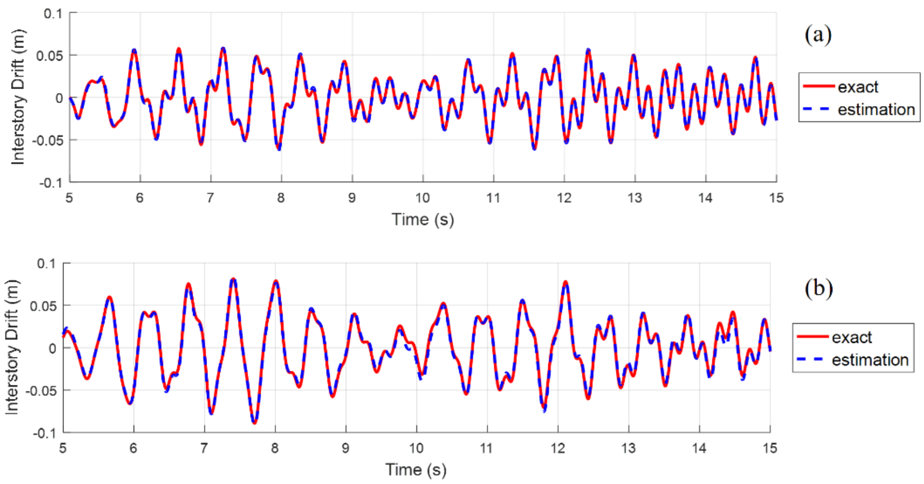

Fig. 11. Comparison with NSKT for (a) interstory drift of first floor and (b) device stroke

Table 5. Estimation errors of the dynamic interstory drifts in the linear 2-story building

Story	El Centro		Non-stationary Kanai-Tajimi	
	Amplitude Error (%)	RMS Error (%)	Amplitude Error (%)	RMS Error (%)
1	2.43	2.34	4.86	2.25
2	0.82	5.71	1.87	3.79
NES	1.78	5.87	1.57	3.51

5. LABORATORY VALIDATION

This section presents a laboratory validation of the proposed method. First, the experimental setup is described. Then, the results and their discussion are presented.

5.1 Experimental setup

A 6-story planar steel frame was excited using a uniaxial shaking table; based on traditional system identification methods, the first frequencies of the frame were 1.63 Hz and 5.13 Hz, and first modal damping ratios are 3.9% and 1.9%. The absolute accelerations were measured using 3 smart wireless sensors Xnodes at floors 4, 5, and 6; the data acquisition was set to 100 Hz. Vision-based measurements were also obtained to extract displacements and used as a reference for comparison. Specifically, a checkerboard pattern was attached to each sensor, visible to the camera and acting as target for tracking. Due to limited size of the pattern (smaller than 4-by-4), the MATLAB toolbox which was used to detect and track the checkerboard pattern was not applicable (Calibrator, 2019). Thus, a simple pattern matching using 2-dimensional cross-correlation was used on each frame to track the displacement of each floor in pixel unit. Then the measurement was converted to mm given the size of each square of the checkerboard pattern was 20 mm x 20 mm. Nikon D3300 camera with the lens of 18-55mm was used, and data acquisition was set to 60 frames-per-second for video recording. Fig. 12 shows the test setup.

Three ground motion records with different dynamic properties were considered as the motion of the shaking table to excite the structure: El Centro 1940, Northridge 1994, and Kobe 1995.

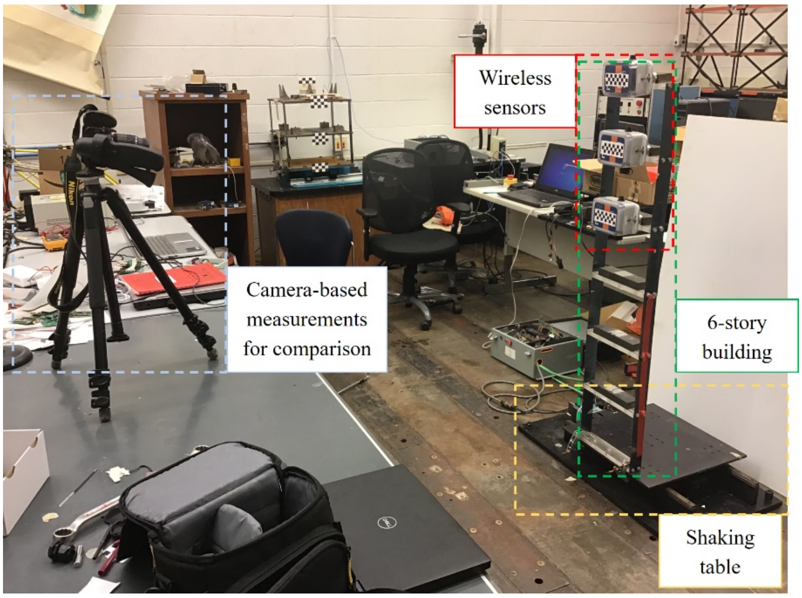

Fig. 12. Experimental setup

5.2 Results and Discussion

The proposed dynamic interstory drift estimation method is applied to the measured accelerations, and it considers the following parameters: $f_s = 100$ Hz, $n = 4$, $f_T = 1.2$ Hz, $\alpha_T = 0.99$, and $N_w = 5.223$. The total interstory drift is considered as a reference for comparison, this is because in the measurements, the pseudo-static components are very small and no need to extract the dynamic counterparts. Fig. 13a-c show the comparison of a time-window of the dynamic interstory drift estimation for floor 5 against the camera-based measurement subjected to all ground motions. It can be demonstrated that the estimated values and the exact values match well for all time steps.

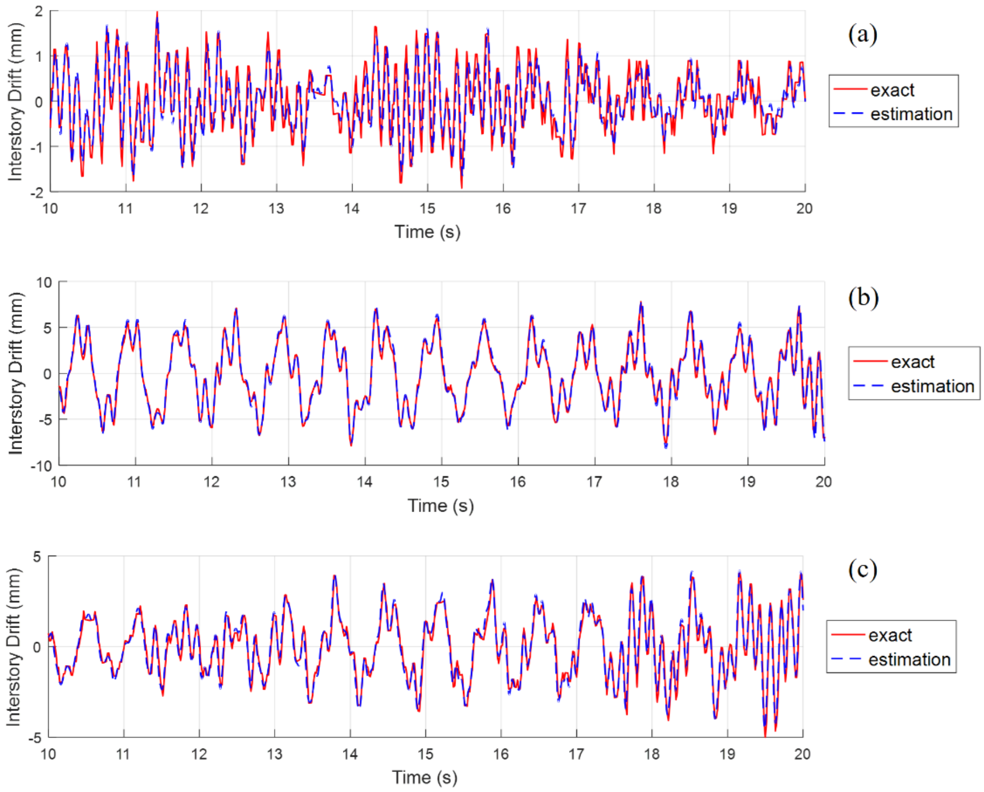

Fig. 13. Comparison of interstory drifts for 5th story (a) El Centro, (b) Northridge, and (c) Kobe earthquakes

The results of the experimental validation for all cases indicate that the proposed interstory drift estimation, such that the maximum magnitude error is smaller than 5.5% for all cases. Table 6 shows the errors in the proposed method compared to camera-based measurements. It is worth noting that the comparison is done against the total interstory drift because the pseudo-static component is negligible. It is concluded that the method is adequate for interstory drift estimation in both amplitude and phase. Currently, many building structures include nonlinear protection devices. As the nonlinearities occur at the discrete locations, where these devices are located, the proposed approach also works well for estimating total interstory drifts in these structures.

Table 6. Estimation errors of the dynamic interstory drifts for laboratory validation

Excitation	Story	Amplitude Error (%)
El Centro	5	4.46
	6	5.10
Northridge	5	5.42
	6	4.74
Kobe	5	5.31
	6	4.24

6. CONCLUSIONS

This paper proposes a new method to estimate dynamic interstory drifts in buildings using measured accelerations from smart wireless sensors. The method uses an effective FIR filter that is suited to better suppress low-frequency noise with small ripple in the passband, based on a minimization problem with Tikhonov regularization. This method then makes use of the difference of the measured acceleration from different floors, which requires the measurements to be time-synchronized. Dynamic interstory drift estimation using acceleration measurements has the potential to be implemented by leveraging WSS. But time synchronization must be addressed first between WSS nodes. A two-point two-stage method to efficiently perform time synchronization of multiple WSS is presented to reduce the errors to exceptionally small values.

The proposed method was demonstrated and evaluated via numerical simulations of both linear and nonlinear hysteretic buildings subjected to ground motions, and subsequently demonstrated in laboratory tests of a small-scale steel frame subjected to different earthquake records. Both numerical and lab test results demonstrate that the proposed method provides a very accurate estimation of the dynamic interstory drifts of buildings.

Future work in this topic will consist in improving the filter by making the window of the filter shorter, such that the lag between the measurement and prediction becomes smaller and implementation is more efficient as fewer arithmetic operations are needed in the WSS. Additionally, the filter will be studied to include an estimation of the pseudo-static interstory drifts in nonlinear structures. Experiments on large-scale buildings will be conducted.

DATA AVAILABILITY STATEMENT

Some data, models, and code that support the findings of this study are available from the corresponding author upon reasonable request.

ACKNOWLEDGEMENTS

The authors want to gratefully acknowledge FRA for the financial support of this research under contract DTFR53-17-C-00007, and ZJU-UIUC Institute Research under Grant #ZJU083650, NTU Start-up Grant 021323-00001, MOE AcRF Tier 1 RG121/21.

REFERENCES

Abé, M. and Fujino, Y. 2017. "Displacement based monitoring of civil structures." *13th International Workshop on Advanced Smart Materials and Smart Structures Technology*, Japan.

Bennett, K.D. and Batroney, C.B. 1997. "Interstory drift monitoring in smart buildings using laser crosshair projection." *Optical Engineering*, 36(7). https://doi.org/10.1117/1.601396

Bocca, M., and Eriksson, L.M. 2011. "A synchronized wireless sensor network for experimental modal analysis in structural health monitoring." *Computer-Aided Civil and Infrastructure Engineering*, 26, 483–499. https://doi.org/10.1111/j.1467-8667.2011.00718.x

Calibrator, C. 2019. "Detect checkerboard pattern in image - MATLAB *detectCheckerboardPoints.*" [online] Mathworks.com. Available at: https://www.mathworks.com/help/vision/ref/detectcheckerboardpoints.html [Accessed 4 Jan. 2019].

Fu, Y., Hoang, T., Mechitov, K., Kim, J.R., Zhang, D., and Spencer Jr, B. F. 2021a. "xShake: Intelligent wireless system for cost-effective real-time seismic monitoring of civil infrastructure." *Smart Structures and Systems*, 28(4), 483-497. https://doi.org/10.12989/sss.2021.28.4.483

Fu, Y., Mechitov, K., Hoang, T., Kim, J.R, Lee, D.H., and Spencer, Jr., B.F. 2019. "Development and full-scale validation of high-fidelity data acquisition on a next-generation wireless smart sensor platform." *Advances in Structural Engineering*, 22(16), 3512-33. https://doi.org/10.1177/1369433219866093

Fu, Y., Mechitov, K., Hoang, T., Kim, J.R., Memon, S.A., and Spencer, Jr., B.F. 2021b. "Efficient and high-precision time synchronization for wireless monitoring of civil infrastructure subjected to sudden events." *Structural Control and Health Monitoring*, 28(1), e2643. https://doi.org/10.1002/stc.2643

Fu, Y., Mechitov, K.A., Hoskere, V., and Spencer, Jr., B.F. 2016. "Development of RTOS-based wireless SHM system: benefits in applications." *International Conference on Smart Infrastructure and Construction*, Cambridge, UK, June 27-29.

Fu, Y., Zhu, L., Hoang, T., Mechitov, K. and Spencer Jr, B.F., 2018. "Demand-based wireless smart sensors for earthquake monitoring of civil infrastructure." In *Sensors and Smart Structures Technologies for Civil, Mechanical, and Aerospace Systems 2018* (10598, 245-251). SPIE.

Gindy, M., Vaccaro, R., Nassif, H., and Velde, J. 2008. "A state-space approach for deriving bridge displacement from acceleration." *Computer-Aided Civil and Infrastructure Engineering*, 23(4), 281-290. https://doi.org/10.1111/j.1467-8667.2007.00536.x

Gomez, F., Fermandois, G.A. and Spencer Jr, B.F., 2021. “Optimal design of nonlinear energy sinks for mitigation of seismic response on structural systems.” *Engineering Structures*, *232*, 111756. https://doi.org/10.1016/j.engstruct.2020.111756

Gomez, F., Park, J.W., and Spencer, B.F. Jr. 2018. “Reference-free structural dynamic displacement estimation method.” *Structural Control and Health Monitoring*, 25, e2209. https://doi.org/10.1002/stc.2209

Hester, D., Browjohn, J., Bocian, M., and Xu, Y. 2017. “Low cost bridge load test: calculating bridge displacement from acceleration for load assessment calculations.” *Engineering Structures*, 143, 358-374. https://doi.org/10.1016/j.engstruct.2017.04.021

Hong, Y.H., Kim, H.K., and Lee, H.S. 2010. “Reconstruction of dynamic displacement and velocity from measured accelerations using the variational statement of an inverse problem.” Journal of Sound and Vibration. 329(23), 4980-5003. https://doi.org.remotexs.ntu.edu.sg/10.1016/j.jsv.2010.05.016

Islam MN, Zareie S, Alam MS, and Seethaler RJ. 2016. “Novel method for interstory drift measurement of building frames using laser-displacement sensors.” *Journal of Structural Engineering*, 142(6), 06016001. https://doi.org/10.1061/(ASCE)ST.1943-541X.0001471

Jo, H., Sim, S.H., Nagayama, T., and Spencer Jr., B.F. 2011. “Development and application of high-sensitivity wireless smart sensors for decentralized stochastic modal identification.” *Journal of Engineering Mechanics*, 138(6), 683-694. https://doi.org/10.1061/(ASCE)EM.1943-7889.0000352

Kim, J., Kim, K., and Sohn, H. 2014. “Autonomous dynamic displacement estimation from data fusion of acceleration and intermittent displacement measurements.” *Mechanical Systems and Signal Processing*, 42(1-2), 194-205. https://doi.org/10.1016/j.ymssp.2013.09.014

Kim, J., Swartz, A., Lynch, J.P., Lee, J.J., and Lee, C.G. 2010. “Rapid-to-deploy reconfigurable wireless structural monitoring systems using extended-range wireless sensors.” *Smart Structures and Systems*, 6(5-6), 505-524. https://doi.org/10.12989/sss.2010.6.5_6.505

Kim, K., Choi, J., Chung, J., Koo, G., Bae, I.H., and Sohn, H. 2018. “Structural displacement estimation through multi-rate fusion of accelerometer and RTK-GPS displacement and velocity measurements.” *Measurement*, 130, 223-35. https://doi.org.remotexs.ntu.edu.sg/10.1016/j.measurement.2018.07.090

Kim, K. and Sohn, H. 2017. “Dynamic displacement estimation by fusing LDV and LiDAR measurements via smoothing based Kalman filtering.” *Mechanical Systems and Signal Processing*, 82(1), 339-355. https://doi.org/10.1016/j.ymssp.2016.05.027

Lee, H.S., Hong, Y.H., and Park, H.W. 2010. “Design of an FIR filter for the displacement reconstruction using measured acceleration in low-frequency dominant structures.”

International Journal for Numerical Methods in Engineering. 82(4), 403-434. https://doi.org/10.1002/nme.2769

Lee, J., Lee, K.C., Jeong, S., Lee, Y.J., and Sim, S.H. 2020. “Long-term displacement measurement of full-scale bridges using camera ego-motion compensation.” *Mechanical Systems and Signal Processing*, 140, 106651. https://doi.org/10.1016/j.ymssp.2020.106651

Liu, C., Park, J.W, Spencer, B.F. Jr., Moon, D.S. and Fan, J. 2017. “Sensor fusion for structural tilt estimation using an acceleration-based tilt sensor and a gyroscope.” *Smart Materials and Structure*, 26(10), 105005. https://doi.org/10.1088/1361-665X/aa84a0

Li, J., Mechitov, K.A., Kim, R.E., and Spencer, Jr. B.F. (2016). “Efficient time synchronization for structural health monitoring using wireless smart sensor networks”, *Structural Control and Health Monitoring*. 23(3), 470-486. https://doi.org/10.1002/stc.1782

Luo, L. and Feng, M.Q. 2018. “Edge-enhanced matching for gradient-based computer vision displacement measurement.” *Computer-Aided Civil and Infrastructure Engineering*, 33(12), 1019-40. https://doi.org/10.1111/mice.12415

Lynch, J.P., and Loh, K.J. 2006. “A summary review of wireless sensors and sensor networks for structural health monitoring.” *Shock and Vibration Digest*, 38(2), 91-130. https://doi.org/10.1177/0583102406061499

Nagayama, T., and Spencer Jr, B.F. 2007. “Structural health monitoring using smart sensors.” Newmark Structural Engineering Laboratory. University of Illinois at Urbana-Champaign.

Nagayama, T., Suzuki, M., Zhang, C., and Su, D. 2017. “High-accuracy wireless sensor development and its application to deflection estimation of a steel box girder bridge.” *13th International Workshop on Advanced Smart Materials and Smart Structures Technology*, Japan.

Pan, H., Yuen, K.V, and Kusunoki, K. 2021. “Displacement estimation for nonlinear structures using seismic acceleration response data.” *Journal of Earthquake Engineering*, 11, 1-9. https://doi.org/10.1080/13632469.2021.1997838

Park, J.W., Moon, D.S., Yoon, H., Gomez, F., Spencer, B.F. Jr., and Kim, J.R. 2018. “Visual–inertial displacement sensing using data fusion of vision-based displacement with acceleration.” *Structural Control and Health Monitoring,* 25, e2122. https://doi.org/10.1002/stc.2122

Park, J.W., Sim, S.H., and Jung, H.J. 2013. “Displacement estimation using multimetric data fusion.” *IEEE/ASME Transactions On Mechatronics*, 18(6), 1675-82. https://doi.org/10.1109/TMECH.2013.2275187

Rawat, P., Singh, K.D., Chaouchi, H., and Bonnin, J.M. 2014. “Wireless sensor networks: a survey on recent developments and potential synergies.” *The Journal of supercomputing*, 68(1), 1-48. https://doi.org/10.1007/s11227-013-1021-9

Rice, J.A., Mechitov, K., Sim, S.H., Nagayama, T., Jang, S., Kim, R., Spencer Jr, B.F., Agha, G., and Fujino, Y. 2010. “Flexible smart sensor framework for autonomous structural health monitoring.” *Smart Structures and Systems*, 6(5-6), 423-438. https://doi.org/10.12989/sss.2010.6.5_6.423

Rice, J.A., Mechitov, K. A., Sim, S.H., Spencer Jr, B.F., and Agha, G.A. 2011. “Enabling framework for structural health monitoring using smart sensors.” *Structural Control and Health Monitoring*, 18(5), 574-587. https://doi.org/10.1002/stc.386

Skolnik, D.A. and Wallace J.W. 2010. “Critical assessment of interstory drift measurements.” *Journal of Structural Engineering*, 136(12), 1574-1584. https://doi.org/10.1061/(ASCE)ST.1943-541X.0000255

Spencer, Jr., B.F., Park, J.W., Mechitov, K.A, Jo, H., and Agha, G. 2017. “Next generation wireless smart sensors toward sustainable civil infrastructure.” *Procedia engineering*, 171, 5-13. https://doi.org./10.1016/j.proeng.2017.01.304

Wang, Y., Lynch, J.P., and Law, K.H. 2007. “A wireless structural health monitoring system with multithreaded sensing devices: design and validation.” *Structure and Infrastructure Engineering*, 3(2), 103-120. https://doi.org/10.1080/15732470600590820

Xu, J., Spencer, B.F. Jr., and Lu, X. 2017. “Performance-based optimization of nonlinear structures subject to stochastic dynamic loading.” *Engineering Structures*, 134, 334-345. https://doi.org/10.1016/j.engstruct.2016.12.051

Xu, J., Spencer, B.F. Jr., Lu, X., Chen, X., and Lu, L. 2017. “Optimization of structures subject to stochastic dynamic loading.” *Computer-Aided Civil and Infrastructure Engineering*, 32(8), 657-673. https://doi.org/10.1111/mice.12274

Zheng, W., Dan, D., Cheng, W., and Xia, Y. 2019. “Real-time dynamic displacement monitoring with double integration of acceleration based on recursive least squares method.” *Measurement*, 141, 460-71. https://doi.org/10.1016/j.measurement.2019.04.053

Zhu, H., Gao, K., Xia, Y., Gao, F., Weng, S., Sun, Y., and Hu, Q. 2020. “Multi-rate data fusion for dynamic displacement measurement of beam-like supertall structures using acceleration and strain sensors.” *Structural Health Monitoring*, 19(2), 520-36. https://doi.org/10.1177/1475921719857043